Investigation of 1.3 μm AlGaInAs multi-quantum wells for electro-absorption modulated laser

Guillaume Binet, Jean Decobert, Nadine Lagay, Nicolas Chimot, Christophe Kazmierski

To cite this version:

Guillaume Binet, Jean Decobert, Nadine Lagay, Nicolas Chimot, Christophe Kazmierski. Investigation of 1.3 μm AlGaInAs multi-quantum wells for electro-absorption modulated laser. Physica Status Solidi A (applications and materials science), 2016, 213 (10), pp.2699-2703 10.1002/pssa.201532729 . hal-01328579

HAL Id: hal-01328579

https://hal.sorbonne-universite.fr/hal-01328579v1

Submitted on 8 Jun 2016

HAL is a multi-disciplinary open access archive for the deposit and dissemination of scientific research documents, whether they are published or not. The documents may come from teaching and research institutions in France or abroad, or from public or private research centers.

L'archive ouverte pluridisciplinaire **HAL**, est destinée au dépôt et à la diffusion de documents scientifiques de niveau recherche, publiés ou non, émanant des établissements d'enseignement et de recherche français ou étrangers, des laboratoires publics ou privés.

Investigation of 1.3 µm AlGaInAs Multi Quantum Wells for Electro-Absorption Modulated Laser

Guillaume Binet[*1,2], Jean Decobert[1], Nadine Lagay[1], Nicolas Chimot[1] and Christophe Kazmierski[1]

[1] III-V Lab, Route de Nozay, F-91461 Marcoussis, France
[2] Institut Jean le Rond d'Alembert, Sorbonne Universités, UPMC Univ Paris 06, CNRS, UMR 7190, F-75005 Paris, France
Keywords III-V semiconductors, AlGaInAs, multiquantum well, electro-absorption modulator, quantum confined Stark effect.

* Corresponding author: e-mail guillaume.binet@3-5lab.fr

Monolithic PIC transmitters using the prefixed optical phase switching concept for BPSK modulation format have been shown promising at 1.55 µm band. These devices could also be crucial for short reach connections and access networks. With this aim, we are studying basic quantum well designs for a laser and an electro-absorption modulator switch to be integrated by selective area growth into PICs at 1.3 µm. Photocurrent measurements and band offset modeling have been performed to determine the MQW stack well-fitted for this application. Broad area laser measurements have also been checked on these structures to verify the material lasing properties. A 6 nm thick well with low barrier seems to be the best trade-off between absorption and shift for 1.3 µm EAM and it also gives good lasing properties.

1 Introduction

With the development of the internet, smart phone applications and cloud computing, the demand for data rate for local area network (LAN) is exploding. Electro-Absorption Modulators (EAM) integrated with a laser or Directly Modulated Lasers (DML) are already used for 10 Gbit and 40 Gbit transmission applications due to their small size and low electrical consumption [1,2]. To address the specifications for 100Gbit and 400Gbit Ethernet, the number of components on chip has to be increased but at the expense of larger footprint, as well as extra cost and electrical consumption. Monolithic integration on InP is a way to facilitate the fabrication of complex Photonic Integrated Circuits (PIC) provided with multiple functions. We have sucessfully shown that InP actually provides the lowest-size full-monolithic transmitters (TX) for complex modulation formats (m-PSK, QAM etc) using a novel prefixed optical phase switching by low drive using EAM [3,4,5]. While keeping simple the transmitter and its driving electronics, it has the advantage over the more standard Pulse Amplitude Modulation (PAM) format to suppress the optical carrier and to provide better energy efficiency [6]. However, up to now, this technique was mostly used to fabricate monolithic transmitters in 1.55 µm band as clear applications for 100 Gb/s long-haul transmissions [7]. However, the small size and low consumption monolithic transmitters appear as an attractive solution for emerging terabit short reach connections and probably for the next speed rise in access network also being very sensitive to costs of terminals. These applications make use of 1.3µm bands for low dispersion of fibre.

With this aim, we are studying basic quantum well design for a laser and an electro-absorption modulator switch to be integrated into Photonic Integrated Circuits (PIC) using our Selective Area Growth (SAG) platform. Optimum design for 1.3 µm imposes new more stringent requirements.

In the first part of this paper, we present our SAG integration platform. Then, we present the trade-off on bandgap and well thickness on the excitonic properties in EAM. We show the MQW design of efficient modulator using AlGaInAs MQWs in the 1.3 µm band. It has been reported that compared to conventional InGaAsP, the quaternary AlGaInAs allows enhanced excitonic effects, a higher bandwidth and high temperature operation [8,9]. We also report on experimental results from several structures and evaluate exciton strength and shift under electric field. Finally we present measurements about basic material lasing performances of the different structures.

2 Photonic integration technology

The EAM integrated with a DFB laser (EML) is a photonic integrated circuit with 3 types of functions which are separated into component sections: continuous wave laser, EAM and passive waveguides for section separation

and optical power. Because EAM is really sensitive to the detuning between the laser emitting wavelength and the modulator absorption edge, optimal bandgap engineering of the optical functions is mandatory.

An integration scheme easily suitable for this purpose is SAG by metal organic vapour phase epitaxy (MOVPE). It is a powerful technique for monolithic integration, where different bandgap materials are defined simultaneously in a single epitaxial growth. It is performed on dielectric patterned substrates. Because the dielectric is amorphous, the active precursors do not nucleate on it, so they diffuse and induce growth variation in the vicinity of the masked zone. Then for any alloy composed of more than twp elements, not only an enhancement of the thickness happens but also a compositional shift due to different decomposition rates of group III element precursors in the vapour phase.

Thus modeling is necessary to design the mask stripes. For quaternary alloys $Al_yGa_xIn_{1-x-y}As$, it is more difficult because three elements III are mixed in the vapor phase. A simple approach to model SAG is to consider only vapor phase diffusion (VPD) as the source material of supply. If no interaction is assumed between group III elements, each binary element can be considered to have an independent growth enhancement ratio that leads to identification of the composition and the growth enhancement ratio of the alloy in the vicinity of the mask [3].

3 Material design

Optimal bandgap engineering is essential to optimize relevant EAM features such as optical saturation intensity, extinction ratio (ER) and modulation efficiency expressed in dB/V. Power saturation phenomena in the EAM is known to be due to a slow carrier sweep-out from the active region resulting in photogenerated low-mobility hole accumulation (pile-up) in the valence band wells [10]. The presence of carriers has different consequences such as field screening and decreased Quantum Confined Stark Effect (QCSE) leading to low ER, large capacitance and so limited bandwidth.
The optical saturation intensity is given by [11]

$$I_S = \frac{\hbar\omega N_S}{\alpha\,(L_w + L_b)}\,\frac{m_e + m_h}{m_e\tau_h + m_h\tau_e} \quad (1)$$

with $\hbar\omega$ the photon energy, N_S the carrier population at saturation, α the absorption coefficient, L_w (L_b) the well (barrier) thickness, m_e (m_h) the electron (hole) effective mass and τ_e (τ_h) the electron (hole) lifetime.

According to (1), the optical saturation intensity is enhanced by reducing the well thickness and the carriers lifetime. However, only the hole lifetime can be taken into consideration because of the difference in effective mass with electrons which are swept out much faster than holes. The latter is given by [11]

$$\tau_h^{-1} \approx \tau_R^{-1} + A_h \exp\left(-\frac{\Delta E_{v,eff}}{k_B T}\right) + B_h \exp\left(-2L_b\sqrt{2m_h\,\Delta E_{v,eff}}\,/\hbar\right) \quad (2)$$

with $\Delta E_{v,eff}$ the effective valence band offset ($\Delta E_v - E_1$) as shown on Figure 1.

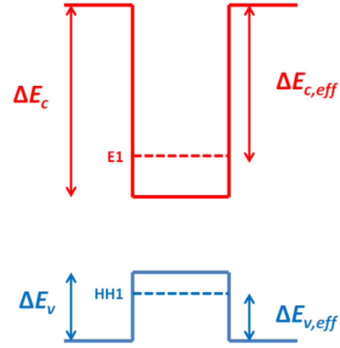

Figure 1 Schematic diagrams of AlGaInAs MQW band diagram with 1% well strain and -0.6 % barrier strain

In (2), the first term is the carrier recombination, the second term the thermionic emission and the third the tunnelling emission [11,12]. It shows that the hole lifetime is reduced with ΔEv,eff.

Furthermore, ER and modulation efficiency are governed by the excitonic absorption. It is therefore important to enlarge the exciton strength and exciton shift ΔE under electric field F so as to benefit from large ER and large modulation efficiency. Firstly, according to [13], ΔE is proportional to the fourth power of the well width (3)

$$\Delta E \propto F^2 L_w{}^4 \quad (3)$$

Increasing ΔE is therefore inconsistent with the optimization of the optical saturation intensity according to (1). It is also inconsistent with the exciton strength enlargement with L_w lowering [14]. However, the exciton strength can be improved by enhancing exciton binding energy by improving carrier confinement through the barrier bandgap increase. Nevertheless it also turns out to be opposite to the optical saturation intensity improvement. These different trade-offs emphasize the relevance of the bandgap engineering.

Moreover, it was demonstrated that highly strained barriers reduce the carrier escape time [15]. Figure 2 shows simulated effective band offset for both electrons and holes from AlGaInAs MQW structures. The barriers are 6nm

thick with different bandgaps and strain and identical 5nm thick wells are used for all the structures.

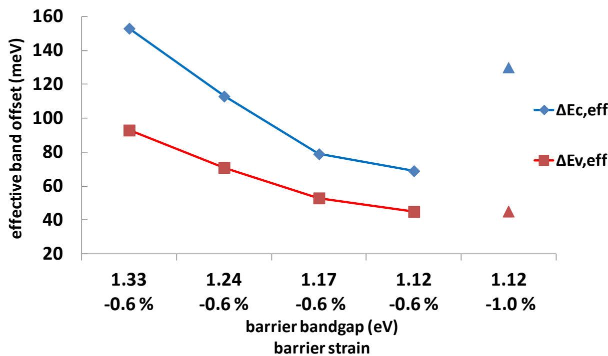

Figure 2 Simulation of $\Delta E_{v,eff}$ and $\Delta E_{c,eff}$ for AlGaInAs MQW of 5 nm well thickness and 6 nm barrier thickness

When the tensile barrier strain is fixed at -0.6%, it can be noticed that when the barrier bandgap is reduced, a low $\Delta E_{v,eff}$ is achieved so as to reduce the hole carrier pile-up and optical saturation. However, the effective conduction band offset is also reduced which can be too detrimental for laser thermal properties. This effect can be addressed by increasing the tensile barrier strain for a 1.12eV barrier bandgap with -1% tensile strain.

4 Characterization results

4.1 Sample structure and fabrication

The crystal growths were carried out by MOVPE. The MQW active layers are undoped and made of compressively strained wells between tensile strained barriers. Seven structures were grown with the same undoped active layer thickness to keep a constant applied electric field and a constant confinement parameter (see Table 1). All the structures are 1% compressively strained well. The structures A and B consist respectively of 8 and 6 nm thick well with $\Delta E_{v,eff}$. The structure C was grown to evaluate the barrier strain influence as described on Figure 2. An example of stack is described in Table 2.

Table 1 Summary chart of the seven structures

Structure	Well thickness	Barrier thickness	$\Delta E_{v,eff}$	Barrier strain
A1			126 meV	
A2	10 x 8 nm	11 x 10 nm	107 meV	-0.6 %
A3			91 meV	
B1			126 meV	
B2	13 x 6 nm	14 x 7.5 nm	98 meV	-0.6 %
B3			70 meV	
C	16 x 5 nm	17 x 6 nm	45 meV	-1 %

Table 2 Schematic of AlGaInAs compressive strained MQW of structure A1

Layer	Composition	Thickness (nm)	doping
p contact	InGaAs	300	p=3x10^{19} (Zn)
spacer	InP	2500	p=1.4x10^{18} (Zn)
SCH	$Al_{39}Ga_{08}In_{53}As$	20	undoped
Barrier	$Al_{0.375}Ga_{0.185}In_{0.440}As$	10	undoped
Well	$Al_{0.166}Ga_{0.174}In_{0.660}As$	8 (x 10)	undoped
Barrier	$Al_{0.375}Ga_{0.185}In_{0.440}As$	10 (x 10)	undoped
SCH	$Al_{39}Ga_{08}In_{53}As$	60	undoped
buffer	InP	2000	n=1x10^{18} (Si)
substrate	InP		

4.2 QSCE measurements

Photocurrent spectra were recorded to access QCSE shift and excitonic absorption strength. The spectra for the structure A1 is shown in Figure 3 as an example. The excitonic peak can be identified around 1265 nm at 0V. The shift and the decrease of the excitonic peak are also clearly visible when the electric field is increased. We reported the relative amplitude and the wavelength shift for all the structures respectively in Figures 4 and 5. In Figure 4, the relative exciton peak height represents the photocurrent of the exciton peak normalized by its value at 0 V.

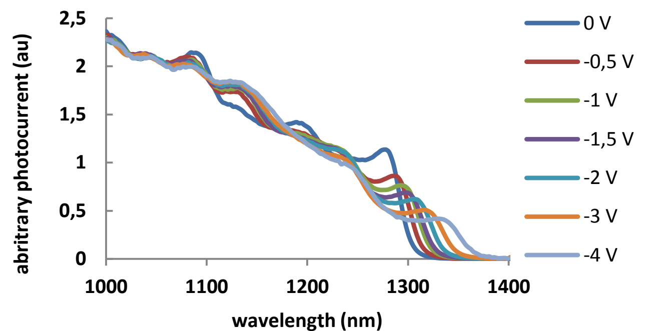

Figure 3 Measured photocurrent spectra for the structure A1

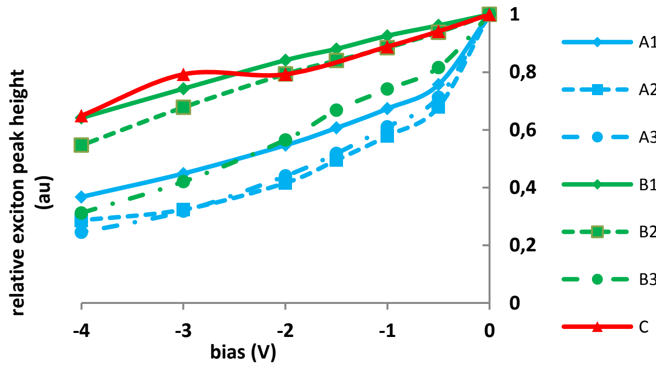

Figure 4 Measured QSCE absorption spectra

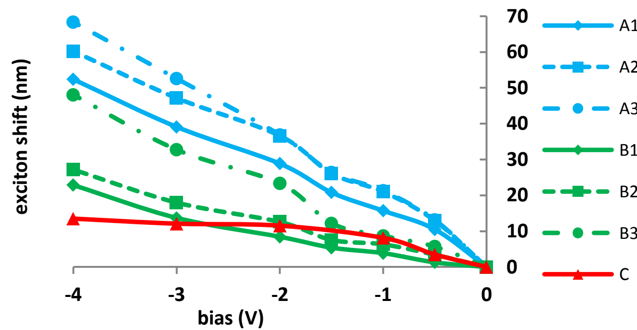

Figure 5 Measured QSCE shift spectra

From Figures 4 and 5, it can be noticed by comparing structures A and B that the first order effect on the exciton strength and shift is the well thickness. Then, the exciton strength and shift trade-off with the well thickness is clearly visible and confirms the expectations described previously. Besides, for a given well thickness, the larger the ΔEv,eff, the higher the exciton strength,and the lower the exciton shifts. This can be explained by a reduction of the barrier bandgap which induces a decrease of the exciton binding energy. The structure B3 (6 nm-thick well and ΔEv,eff of 70 meV) presents a lower excitonic strength while having a higher exciton shift and differs clearly from structures B1 and B2 with higher ΔEv,eff.

In the case of structure B3, only one heavy hole level is confined in the valence band. The field screening is thereby reduced but the excitonic strength is also reduced due to a decreased exciton binding energy.The specific 5 nm-thick well structure C was grown with 1 % tensile strain barrier and presents a ΔEv,eff of 45 meV. The objective was to reduce the offset to increase the exciton shift and keep a large effective conduction band offset. Thus, from 0 to 2V under inverted bias, the shift is comparable to the 6 nm well structures with an ΔEv,eff of 98 meV and 128 meV. This demonstrates the relevance of strain engineering to reach low ΔEv,eff with narrow wells while keeping a large effective conduction band offset and opens the path to refine band structure design.

4.3 Broad area laser characteristics

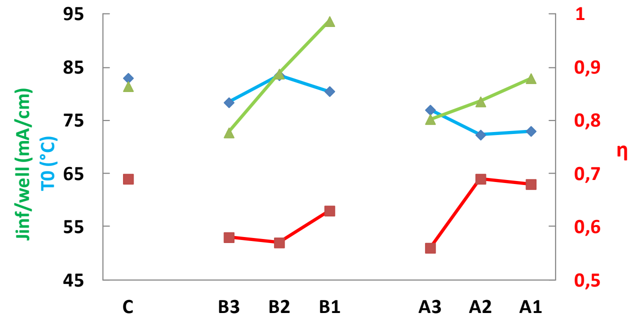

Figure 6 Summary of the threshold current density J_{inf}/well (green), the characteristics temperature T_0 (blue) and the internal quantum efficiency (red) for the different structures

To verify the quality of the material in terms of lasing performance, broad area (BA) lasers are generally fabricated. They are used to evaluate the threshold current density for an infinite ridge J_{inf}/well, the internal quantum efficiency η and the characteristic temperature T_0 and this has been done for the seven structures.

Thus, for J_{inf}/well, the average behaviour of the different structures is comparable, except that for a given well thickness the threshold decreases with the barrier height. Then, the internal quantum efficiency of the different structures are alike and characteristic temperature is better for thinner wells.

In consequence by using SAG, it is possible to tune the laser bandgap to use the optimal detuning.

5 Summary and conclusion

Discrete or small scale PIC transmitting components, especially those based on indium phosphide technology, have become an integral part of the optical fiber communication industry. In this context, InP-based quantum well electro-absorption modulators (EAMs) emerge as ones of the smallest (<100µm waveguide length) and most energy-efficient electro-optic converters.

In this paper, we presented the influence of well thickness and barrier bandgap on AlGaInAs-based MQW EAM performances and BA laser performances. This work gives paramount information on EAM design and compares the influence of some material parameters in terms of absorption. It also shows the possibility of integrating the EAM with a laser by SAG, as the BA performances are sufficient.

Structures for efficient modulators show best trade-offs with a 6 nm well thickness structure with the lower barrier.

Acknowledgements

Part of this work was supported by the Ministry of Industry STEAM project and the Nano2017 program.

References

[1] W. Kobayashi, T. Fujisawa, S. Kanazawa and H. Sanjoh, IEEE Electronics Letters, **50**, 299-300 (2014).
[2] H. Klein, C. Bornholdt, G. Przyrembel, A. Sigmund, W-D Molzow, H-G Bach and M. Moehrle., in Proceedings of ECOC 2013, London, Th.1.B.5.
[3] N. Dupuis, J. Decobert, P.-Y. Lagrée, N. Lagay, F. Poingt, C Kazmierski, A. Ramdane and A. Ougazzaden, J. Appl. Phys. **103**, 113113 (2008).
[4] I. Kang, Opt. Express, Vol. 15, No. 4, 1467–1473 (2007).
[5] H. Mardoyan, O. Bertran-Pardo, P. Jennevé, G. De Valicourt, M.A. Mestre, S. Bigo, C. Kazmierski, N. Chimot, A.G. Steffan, J. Honecker, R. Zhang, P. Runge, A. Richter, C. Arellano, A. Ortega-Monux and I. Molina-Fernandez, "in Proceedings of OFC, Th5C.2 (post-deadline), San Francisco (2014).
[6] C. Kazmierski, J. Opt. Commun. Netw. vol. 4, no. 9, A8-A16 (2012).
[7] G. De Valicourt, M. A. Mestre, P. Jennevé, H. Mardoyan, J. C. Antona et al., in Proceedings of OFC, Th5C.3 (post-deadline), San Francisco (2014).
[8] S. J. Sweeney, T. Higashi, A. Andreev, A. R. Adams, T. Uchida and T. Fujii, Phys. Status Solidi B **223**, 573-579 (2001).
[9] W. Kobayashi, M. Arai, T. Yamanaka, N. Fujiwara, T. Fujisawa, T. Tadokoro, K. Tsuzuki, Y. Kondo and F. Kano, J. Lightw. Technol. **28**, 164-171 (2010).
[10] T. Ido, H. Sano, S. Tanaka and H. Inoue, IEEE Phot. Technol. Lett. **7**, 1421-1423 (1995).
[11] A.M. Fox, D.A.B. Miller, G. Livescu, J.E. Cunningham, J.E.Henry and W.Y. Jan, Appl. Phys. Lett. **57** 2315-2317 (1990).
[12] T.H. Wood, J. Pastalan, C. A. Burrus, B. C. Johnson, B. I. Miller, J. L. deMiguel, U. Koren and M. G. Young, Appl. Phys. Lett. **57**, 1081-1083 (1990).
[13] G. Bastard, E.E. Mendez, L.L. Chang and L. Esaki, Phys. Rev. B **26**, 3241-3245 (1983).
[14] S. Schmitt-Rink, S. Chemla, W.H. Knox and D.A.B. Miller, Opt. Lett. **15**, 60-62 (1990).
[15] S. Bouchoule, C. Kazmierski, D. Mathoorasing, A. Ougazzaden and J.-Y. Marzin, IEEE J. of Sel. Top. In Quantum Electron. **3**, 330-335 (1997).